This paper first appeared in the sixteenth print edition of the *Photovoltaics International* journal, published in May 2012.

Predicted thermal stresses in a photovoltaic module (PVM)

E. Suhir, University of California, Santa Cruz, California, **D. Shangguan**, Flextronics Corporation, Milpitas, California, USA, & **L. Bechou**, IMS Laboratory, University of , Bordeaux, Bordeaux, France

ABSTRACT

Low-temperature thermal stresses in a manufactured photovoltaic module (PVM) based on crystalline silicon (Si), before the PVM is fastened into a metal frame, are assessed using a simple, easy-to-use and physically meaningful analytical (mathematical)predictive model. The PVM considered comprises the front glass, ethylene vinyl acetate (EVA) encapsulant (with silicon cells embedded into it) and a laminate backsheet. The stresses addressed include normal stresses that act in the cross sections of the constituent materials and determine their short- and long-term reliability, as well as the interfacial (shearing and peeling) stresses that affect the assembly's ability to withstand delaminations. The interfacial stresses determine also the cohesive strength of the encapsulant. The calculated data, indicate that the induced stresses can be rather high, especially the peeling stress at the encapsulant-glass interface, so that the structural integrity of the module might be compromised, unless the appropriate design-for-reliability (DfR) measures, including stress prediction and accelerated stress testing, are taken. The authors are convinced that reliability assurance of a photovoltaic (PV) product cannot be delayed until it is manufactured – such an assurance should be considered and secured, first of all, at the design stage.

Introduction

The reliability of a product – including a photovoltaic (PV) product (Fig. 1), whether it is crystalline or a thin-film device (Fig. 2) – is conceived at its design stage and implemented during its manufacturing. The reliability should be evaluated and qualified by testing, and, if necessary and appropriate, maintained in the field during the product's operation. It is the general consensus that if reliability is taken care of at the design phase, the final cost of the product is minimal. If a reliability problem is detected during engineering, the cost of the product goes up by an order of magnitude; if the problem is caught at the production stage, the cost of the product might increase by orders of magnitude. In other words, the product's reliability is too important to be left to the stage when it has already been fabricated – it is too late to change anything at such a late stage.

> "The product's reliability is too important to be left to the stage when it has already been fabricated."

Elevated thermal stresses are viewed – along with high humidity, UV radiation and other stresses [1–4] – as the major contributor to the finite lifetime of a photovoltaic module (PVM) [5–7], so it takes place in other electronics and photonics systems (see, for example, Schubert et al. [8] and Lau [9]). In the realization that design-for-reliability (DfR) effort is imperative for minimizing the risk that the PV product will not meet the reliability requirements, objectives and expectations, we address in our analysis, an important situation in the manufacturing process of a crystalline silicon (Si) -based module – the low-temperature thermally induced stresses.

Thermal stress failures can be predicted and prevented effectively, provided that adequate predictive modelling, confirmed and validated by field data, is widely and consistently used in addition (and preferably prior) to experimental investigations and reliability testing [10]. Analytical modelling occupies a special place in the modelling effort [11–14]. Not only is such modelling able to clearly indicate the roles of various factors affecting the behaviour of the design of interest, but, more importantly, it is also often able to better explain the reliability physics behind the product performance than finite-element analyses (FEA) and even the experimentation.

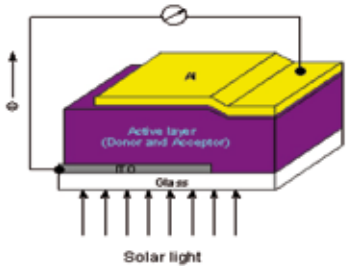

Figure 1. Typical PV device.

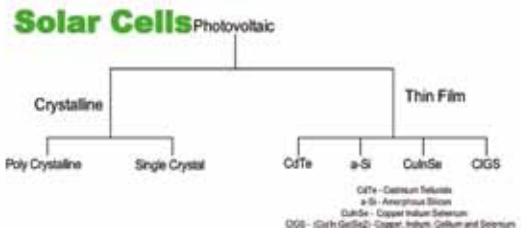

Credit: Green Econometrics – Wanasa Holdings Company LLC

Figure 2. Solar cell (PV) devices.

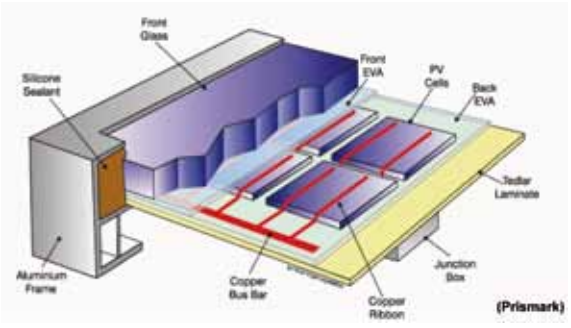

Figure 3. Typical crystalline Si PVM (Prismark).

Accordingly, in the following analysis, an easy-to-use and physically meaningful analytical stress model is developed for evaluating the low-temperature thermal stresses in a crystalline-Si-based PVM (assembly) before it is fastened into a metal frame. The assembly considered comprises the front glass, ethylene vinyl acetate (EVA) encapsulant (with PV silicon cells embedded into it) and a laminate backsheet. The analysis is carried out considering a PVM as shown in Fig. 3.

Figure 4. Tri-material PV-module schematics.

"Thermal stress failures can be predicted and prevented effectively, provided that adequate predictive modelling, confirmed and validated by field data, is widely and consistently used."

Analysis

Assumptions

- A structural analysis (strength-of-materials) approach can be applied for the evaluation of the bow and the stresses. As long as this approach is used, no singular stresses can possibly occur. From the theory-of-elasticity standpoint, the predicted stresses can be viewed as suitable design parameters that characterize the state of stress at the assembly edges.
- The assembly constituents (components) can be treated as thin, elongated plates, experiencing small deflection, so that the engineering theory of such plates (see, for example, Suhir [15]) can be employed.
- The interfacial shearing stresses and the assembly curvature can be evaluated without considering the effect of the peeling stresses; the latter stresses can be subsequently determined from the evaluated shearing stresses and the curvature.
- Thermal stresses caused by the interaction of the dissimilar EVA and Si materials within the inhomogeneous (composite) encapsulant do not have to be considered when evaluating the forces acting in the PVM components, including the thermally induced force in the inhomogeneous encapsulant itself. These forces can be evaluated by assessing and considering the effective mechanical characteristics – Young's modulus, Poisson's ratio, coefficient of thermal expansion (CTE) – of the EVA-Si composite.
- The above-mentioned stresses caused by the interaction of the dissimilar EVA and Si materials within the inhomogeneous (composite) EVA encapsulant can be evaluated from the computed force acting in the EVA-Si composite. This force is considered to be an external mechanical force applied to the EVA-Si composite layer.
- It is assumed that there might not be a good adhesion between the butt ends of the Si device and the EVA, so that the interaction of these materials is due only to their interfacial interaction. This seems to be a reasonable, and certainly a conservative, assumption.

Normal stresses in the assembly mid-portion

The mid-portion addressed (Fig. 4) consists of component 1 (glass), component 2 (encapsulant with the embedded Si devices) and component 3 (backsheet). The equations of compatibility of the longitudinal thermally induced strains in such a tri-material assembly (that has been fabricated at an elevated temperature and subsequently cooled down to a low temperature) can be written as

$$-\alpha_1\Delta t+\lambda_1 T_1^0=-\alpha_2\Delta t+\lambda_2 T_2^0=-\alpha_3\Delta t+ \quad (1)$$

where $\alpha_i, i=1,2,3$, are the CTEs of the materials; Δt is the change in temperature from the manufacturing temperature to the low temperature of interest; $\lambda_i=\frac{1}{E_i^* h_i}, i=1,2,3,$ are the axial compliances of the materials; $E_i^*=\frac{E_i}{1-\nu_i}, i=1,2,3,$ are their effective Young's moduli(that consider the two-dimensional state of stress); $E_i, i=1,2,3$, are the actual Young's moduli of the materials (in the case of the encapsulant composite, it is the modulus of the composite, considering the EVA and Si moduli); $\nu_i, i=1,2,3$, are Poisson's ratios; $h_i, i=1,2,3$, are the layer thicknesses; and $T_i^0, i=1,2,3$, are the thermally induced forces caused by the dissimilar materials in the assembly. The first terms in the expressions of Equation 1 are stress-free (unrestricted) thermal contractions, and the second terms are displacements caused by the thermal forces. In addition to the strain compatibility conditions given in Equation 1, by using the equilibrium condition

$$T_1^0+T_2^0+T_3^0=0\,, \quad (2)$$

the following expressions for the induced forces are obtained:

$$\left.\begin{aligned} T_1^0&=\frac{\lambda_2(\alpha_1-\alpha_3)+\lambda_3(\alpha_1-\alpha_2)}{\lambda_1\lambda_2+\lambda_2\lambda_3+\lambda_3\lambda_1}\Delta t,\\ T_2^0&=\frac{\lambda_3(\alpha_2-\alpha_1)+\lambda_1(\alpha_2-\alpha_3)}{\lambda_1\lambda_2+\lambda_2\lambda_3+\lambda_3\lambda_1}\Delta t\\ T_3^0&=\frac{\lambda_1(\alpha_3-\alpha_2)+\lambda_2(\alpha_3-\alpha_1)}{\lambda_1\lambda_2+\lambda_2\lambda_3+\lambda_3\lambda_1}\Delta t \end{aligned}\right\} \quad (3)$$

The stresses acting in the components' cross sections can be found by dividing the forces in Equations 3 by the thickness of the corresponding component.

Interfacial shearing stresses

Basic equations

The longitudinal interfacial displacements of the assembly components can be expressed, in accordance with the assumptions taken, by the formulas:

$$\left.\begin{aligned} u_{11}(x)&=-\alpha_1\Delta t x+\lambda_1\int_0^x T_1(\xi)d\xi-\kappa_1\tau_1(x)+\frac{h_1}{2}w'(x)\\ u_{21}(x)&=-\alpha_2\Delta t x+\lambda_2\int_0^x T_2(\xi)d\xi+\kappa_2\tau_1(x)-\frac{h_2}{2}w'(x)\\ u_{22}(x)&=-\alpha_2\Delta t x+\lambda_2\int_0^x T_2(\xi)d\xi+\kappa_2\tau_2(x)+\frac{h_2}{2}w'(x)\\ u_{32}(x)&=-\alpha_3\Delta t x+\lambda_3\int_0^x T_3(\xi)d\xi-\kappa_3\tau_2(x)-\frac{h_3}{2}w'(x) \end{aligned}\right\} \quad (4)$$

where $u_{11}(x)$ is the displacement of component 1 (glass) at its interface 1 with component 2 (encapsulant); $u_{21}(x)$ is the displacement of component 2 (encapsulant) at interface 1; $u_{22}(x)$ is the displacement of component 2 (encapsulant) at its interface 2 with component 3 (backsheet); $u_{32}(x)$ is the displacement of the component 3 (backsheet) at interface 2; and Δt is the change in temperature (from the manufacturing temperature to the low temperature of interest). Also,

$$\kappa_1=\frac{h_1}{3G_1},\qquad \kappa_2=\frac{h_2}{G_2},\qquad \kappa_3=\frac{h_3}{3G_3} \quad (5)$$

are the interfacial compliances of the components [16];

$$T_1(x)=\int_{-\ell}^{x}\tau_1(\xi)d\xi\,,\quad T_2(x)=-[T_1(x)+T_3(x)]\,,\quad T_3(x)=\int_{-\ell}^{x}\tau_2(\xi)d\xi \quad (6)$$

are the thermally induced forces acting in the components' cross sections; G_i, i = 1, 2, 3, are the shear moduli of the materials; ℓ is half the assembly length; $\tau_i(x)$, i = 1, 2, is the interfacial shearing stress at the i^{th} interface; and $w(x)$ is the deflection of the assembly. The origin '0' of the longitudinal coordinate x is at the mid-cross section of the assembly in the mid-plane of the intermediate component 2 (encapsulant).

The conditions $u_{11}(x) = u_{21}(x)$ and $u_{22}(x) = u_{32}(x)$ of the compatibility of the interfacial displacements lead to the following equations for the thus-far unknown axial (longitudinal) forces $T_i(x)$, i = 1, 2, 3:

$$\left.\begin{aligned} (\lambda_1+\lambda_2)\int_0^x T_1(\xi)d\xi+\lambda_2\int_0^x T_3(\xi)d\xi-\kappa_{12}\tau_1(x)+\frac{h_1+h_2}{2}w'(x)&=(\alpha_1-\alpha_2)\Delta t x\\ \lambda_2\int_0^x T_1(\xi)d\xi+(\lambda_2+\lambda_3)\int_0^x T_3(\xi)d\xi-\kappa_{23}\tau_2(x)-\frac{h_2+h_3}{2}w'(x)&=(\alpha_3-\alpha_2)\Delta t x \end{aligned}\right\} \quad (7)$$

where

$$\kappa_{12}=\kappa_1+\kappa_2\,,\quad \kappa_{23}=\kappa_2+\kappa_3 \quad (8)$$

are the interfacial compliances of the interfaces 1 (between the glass and the encapsulant) and 2 (between the encapsulant and the backsheet), respectively.

The equations of bending of the assembly components can be written as follows:

$$D_1w''(x)=\frac{h_1}{2}T_1(x)\,,\quad D_2w''(x)=\frac{h_2}{2}[T_1(x)-T_3(x)]\,,\quad D_3w''(x)=-\frac{h_3}{2}T_3(x) \quad (9)$$

where

$$D_i=\frac{E_i h_i^3}{12(1-\nu_i^2)}=\frac{E_i^* h_i^3}{12},\quad i=1,2,3 \quad (10)$$

are the flexural rigidities of the assembly components. Summing up Equations 9, we have

$$Dw''(x)=\frac{h_1+h_2}{2}T_1(x)-\frac{h_2+h_3}{2}T_3(x) \quad (11)$$

where $D = D_1 + D_2 + D_3$. Differentiating Equations 9 with respect to the coordinate x and substituting the expression for the curvature $w''(x)$ determined from Equation 11 into the obtained relationships, the following equations for the unknown distributed forces $T_1(x)$ and $T_3(x)$ are obtained:

$$\left.\begin{aligned} \kappa_{12}T_1''(x)-\lambda_{11}T_1(x)+\lambda_{13}T_3(x)&=-(\alpha_1-\alpha_2)\Delta t\\ \kappa_{23}T_3''(x)-\lambda_{33}T_3(x)+\lambda_{13}T_1(x)&=-(\alpha_3-\alpha_2)\Delta t \end{aligned}\right\} \quad (12)$$

where the axial compliances

$$\left.\begin{aligned} \lambda_{11}&=\frac{(h_1+h_2)^2}{4D}+\lambda_1+\lambda_2\,,\\ \lambda_{33}&=\frac{(h_2+h_3)^2}{4D}+\lambda_2+\lambda_3\,,\\ \lambda_{13}&=\frac{(h_1+h_2)(h_2+h_3)}{4D}-\lambda_2 \end{aligned}\right\} \quad (13)$$

take into account the effect of the flexural rigidity D of the assembly.

Equations 13 indicate that the consideration of the finite flexural rigidity of the assembly results in higher axial compliances. The solutions to Equations 12 must satisfy the zero boundary conditions

$$T_1(\ell) = T_3(\ell) = 0 \tag{14}$$

These conditions consider that no external axial forces are applied at the end cross sections of the assembly. After the forces $T_1(x)$ and $T_3(x)$ are found, the interfacial shearing stresses $\tau_1(x)$ and $\tau_2(x)$ can be determined, by differentiation, from the first and the third formulas of Equations 6:

$$\tau_1(x) = T_1'(x), \qquad \tau_2(x) = T_3'(x) \tag{15}$$

Separating the functions $T_1(x)$ and $T_3(x)$ in Equations 12, we obtain the following two inhomogeneous differential equations

$$\left.\begin{aligned} T_1^{IV}(x) - (k_1^2 + k_2^2)T_1''(x) + \gamma k_1^2 k_2^2 T_1(x) &= \gamma k_1^2 k_2^2 T_1^0 \\ T_3^{IV}(x) - (k_1^2 + k_2^2)T_3''(x) + \gamma k_1^2 k_2^2 T_3(x) &= \gamma k_1^2 k_2^2 T_3^0 \end{aligned}\right\} \tag{16}$$

where the notations:

$$k_1 = \sqrt{\frac{\lambda_{11}}{\kappa_{12}}}, \quad k_2 = \sqrt{\frac{\lambda_{33}}{\kappa_{23}}}, \quad \gamma = 1 - \frac{\lambda_{13}^2}{\lambda_{11}\lambda_{33}} \tag{17}$$

are used. The forces T_1^0 and T_3^0 acting in the mid-portion of the assembly are expressed by the first and the third formulas in Equations 3.

Parameter of the interfacial shearing stresses

The homogeneous equation

$$T^{IV}(x) - (k_1^2 + k_2^2)T''(x) + \gamma k_1^2 k_2^2 T(x) = 0 \tag{18}$$

that corresponds to the two inhomogeneous differential Equation 16 turns out to be the same for both of those equations. The characteristic equation

$$k^4 - (k_1^2 + k_2^2)k^2 + \gamma k_1^2 k_2^2 = 0 \tag{19}$$

leads to the following formula

$$k = \sqrt{\frac{k_1^2 + k_2^2}{2}\left[1 + \sqrt{1 - \gamma\left(\frac{2k_1k_2}{k_1^2 + k_2^2}\right)^2}\right]} \tag{20}$$

for the parameter k of the interfacial shearing stress. Here k_1 and k_2 are the parameters of the shearing stresses $\tau_1(x)$ and $\tau_2(x)$, in the case of a bi-material assembly consisting of components 1 and 2, or of components 2 and 3, respectively. Indeed, the case of a bi-material assembly consisting of components 1 and 2 can be obtained by assuming infinitely large compliance of interface 2 ($k_{23} \to \infty$). The second formula in Equations 17 then results in a zero k_2 value, and Equation 20 yields $k = k_1$. Similarly, the result for the case of an assembly comprising components 2 and 3 can be obtained by letting $k_{12} \to \infty$ in Equations 17 and 20. Consequently, as follows from the first formula in Equations 17, $k_1 = 0$, and Equation 20 yields $k = k_2$.

Axial forces at the assembly ends

The particular solutions to the two inhomogeneous differential equations (Equations 16) are $T_1(x) = T_1^0$ and $T_3(x) = T_3^0$, respectively. These solutions are the thermally induced forces in the mid-portion of the assembly. Considering that the functions $T_1(x)$ and $T_3(x)$ should be symmetric with respect to the mid-cross section ($x = 0$), the general solutions to the differential Equation 16 could be sought as

$$T_1(x) = C_1 \cosh kx + T_1^0, \quad T_3(x) = C_3 \cosh kx + T_3^0 \tag{21}$$

where C_1 and C_3 are constants of integration. The conditions expressed by Equation 14 yield:

$$C_1 = -\frac{T_1^0}{\cosh k\ell}, \qquad C_3 = -\frac{T_3^0}{\cosh k\ell}, \tag{22}$$

so that the distributed longitudinal forces $T_1(x)$ and $T_3(x)$ acting in the cross sections of components 1 and 3 are

$$T_1(x) = T_1^0\left(1 - \frac{\cosh kx}{\cosh k\ell}\right), \qquad T_3(x) = T_3^0\left(1 - \frac{\cosh kx}{\cosh k\ell}\right) \tag{23}$$

The force $T_2(x)$ acting in the encapsulant composite (component 2) can then be determined as

$$T_2(x) = -[T_1(x) + T_3(x)] = T_2^0\left(1 - \frac{\cosh kx}{\cosh k\ell}\right) \tag{24}$$

where the force T_2^0 acting in the mid-portion of a large assembly is given by the second formula in Equations 3.

Predicted interfacial shearing stresses

By taking into account Equations 23 for the distributed longitudinal forces, the interfacial shearing stresses $\tau_i(x)$, i = 1, 2, can be determined, by differentiation, from Equations 15:

$$\tau_1(x) = T_1'(x) = -kT_1^0 \frac{\sinh kx}{\cosh k\ell}, \qquad \tau_2(x) = T_3'(x) = -kT_3^0 \frac{\sinh kx}{\cosh k\ell} \tag{25}$$

Peeling stresses

Basic equations

In order to obtain the governing equations for the interfacial peeling stresses $p_1(x)$ and $p_2(x)$ (the interfacial normal stresses acting in the through-thickness direction of the assembly), account should be taken of the fact that the deflection functions $w_i(x)$, i = 1, 2, 3, of the assembly components are somewhat different. In the following analysis it is assumed that these functions should satisfy the following conditions of compatibility:

$$w_1(x) - w_2(x) = \delta_{12}p_1(x), \qquad w_2(x) - w_3(x) = \delta_{23}p_2(x) \tag{26}$$

where δ_{12} and δ_{23} are the interfacial through-thickness compliances of the assembly components. These compliances can be determined experimentally, or estimated using the following approximate formulas:

$$\delta_{12} = \frac{h_1}{E_1^*} + \frac{h_2}{2E_2^*}, \qquad \delta_{23} = \frac{h_3}{E_3^*} + \frac{h_2}{2E_2^*} \tag{27}$$

The equations of bending (Equations 9) should also be modified. With consideration of the peeling stresses $p_i(x)$, i = 1, 2, and different deflection functions $w_i(x)$, i = 1, 2, 3, of the assembly components, these three equations could be written as

$$\left.\begin{aligned} D_1 w_1''(x) &= \frac{h_1}{2}T_1(x) - \int_{-\ell}^{x}\int_{-\ell}^{x} p_1(\xi)d\xi d\xi' \\ D_2 w_2''(x) &= \frac{h_2}{2}[T_1(x) - T_3(x)] + \int_{-\ell}^{x}\int_{-\ell}^{x} [p_1(\xi) - p_2(\xi)]d\xi d\xi' \\ D_3 w_3''(x) &= -\frac{h_3}{2}T_3(x) + \int_{-\ell}^{x}\int_{-\ell}^{x} p_2(\xi)d\xi d\xi' \end{aligned}\right\} \tag{28}$$

The first terms on the right-hand side of these equations are due to the axial thermally induced forces; the second terms are the bending moments due to the peeling stresses. Eliminating the deflection functions $w_i(x)$, i = 1, 2, 3, from Equations (26) and (28), the following equations for the peeling stress functions $p_i(x)$, i = 1, 2, can be obtained:

$$\left.\begin{aligned} p_1^{IV}(x) + 4s_1^4 p_1(x) - \frac{p_2(x)}{\delta_{12}D_2} &= \frac{h_1D_2 - h_2D_1}{2\delta_{12}D_1D_2}\tau_1'(x) + \frac{h_2}{2\delta_{12}D_2}\tau_2'(x) \\ p_2^{IV}(x) + 4s_2^4 p_2(x) - \frac{p_1(x)}{\delta_{23}D_2} &= \frac{h_3D_2 - h_2D_3}{2\delta_{23}D_2D_3}\tau_2'(x) + \frac{h_2}{2\delta_{23}D_2}\tau_1'(x) \end{aligned}\right\} \tag{29}$$

where

$$s_1 = \sqrt[4]{\frac{D_1 + D_2}{4\delta_{12} D_1 D_2}}, \qquad s_2 = \sqrt[4]{\frac{D_2 + I}{4\delta_{23} D_2}} \tag{30}$$

are parameters of the interfacial peeling stresses of bi-material assemblies consisting of components 1 and 2, and components 2 and 3, respectively. From Equations 28 we find, by differentiation,

$$\left.\begin{aligned} D_1 w_1^{IV}(x) &= -\frac{h_1}{2}\tau_1'(x) - p_1(x) \\ D_2 w_2^{IV}(x) &= -\frac{h_2}{2}[\tau_1'(x) - \tau_2'(x)] + p_1(x) - p_2(x) \\ D_3 w_3^{IV}(x) &= \frac{h_3}{2}\tau_2'(x) + p_2(x) \end{aligned}\right\} \tag{31}$$

As evident from these equations, the lateral loadings acting on components 1 and 3 are

$$q_1(x) = -\frac{h_1}{2}\tau_1'(x) - p_1(x), \qquad q_2(x) = \frac{h_3}{2}\tau_2'(x) + p_2(x) \tag{32}$$

and are due to both peeling and shearing interfacial stresses. Since no loadings other than $q_i(x)$, i = 1, 2, act in the through-thickness direction of the assembly, these loadings must be self-equilibrated:

$$\int_0^\ell q_i(x)dx = 0, \qquad \int_0^\ell \int_0^x q_i(\xi)d\xi d\xi' = 0, \qquad i = 1, 2 \tag{33}$$

Equations 32 and the conditions in Equations 33 therefore result in the following equilibrium conditions for the peeling stress functions $p_i(x)$, i = 1, 2:

$$\int_0^\ell p_i(x)dx = 0, \int_0^\ell \int_0^x p_i(\xi)d\xi d\xi' = 0, \quad i = 1,2 \tag{34}$$

These conditions indicate that the peeling stress loading should be self-equilibrated as well.

Parameter of the peeling stresses

After separating the functions $p_i(x)$, i = 1, 2, in Equations 29, we obtain the following two equations of the eighth order for the interfacial peeling stresses acting at the two interfaces:

$$\left.\begin{aligned} p_1^{VIII}(x) + 4(s_1^4 + s_2^4)p_1^{IV}(x) + \delta p_1(x) &= \frac{h_1 D_2 - h_2 D_1}{2\delta_{12} D_1 D_2}\tau_1^V(x) + \\ &+ \frac{h_1(D_2 + D_3) - h_2 D_1}{2\delta_{12}\delta_{23} D_1 D_2 D_3}\tau_1'(x) + \frac{h_2}{2\delta_{12} D_2}\tau_2^V(x) + \frac{h_2 + h_3}{2\delta_{12}\delta_{23} D_2 D_3}\tau_2'(x) \\ p_2^{VIII}(x) + 4(s_1^4 + s_2^4)p_2^{IV}(x) + \delta p_2(x) &= \frac{h_3 D_2 - h_2 D_3}{2\delta_{23} D_2 D_3}\tau_2^V(x) + \\ &+ \frac{h_3(D_1 + D_2) - h_2 D_3}{2\delta_{12}\delta_{23} D_1 D_2 D_3}\tau_2'(x) + \frac{h_2}{2\delta_{23} D_2}\tau_1'(x) + \frac{h_1 + h_2}{2\delta_{12}\delta_{23} D_1 D_2}\tau_1'(x) \end{aligned}\right\} \tag{35}$$

where

$$\delta = \frac{D}{\delta_{12}\delta_{23} D_1 D_2 D_3} \tag{36}$$

The solution to the homogeneous equation

$$p^{VIII}(x) + 4(s_1^4 + s_2^4)p^{IV}(x) + \delta p(x) = 0 \tag{37}$$

can be sought in the form

$$p(x) = C_0 V_0(sx) + C_2 V_2(sx) \tag{38}$$

Here, C_0 and C_2 are the constants of integration, s is the unknown parameter of the interfacial peeling stress and the functions $V_i(sx)$, i = 0, 1, 2, 3, are expressed as

$$\left.\begin{aligned} V_0(sx) &= \cosh sx \cos sx, \quad V_1(sx) = \frac{1}{\sqrt{2}}(\cosh sx \sin sx + \sinh sx \cos sx) \\ V_2(sx) &= \sinh sx \sin sx, \quad V_3(sx) = \frac{1}{\sqrt{2}}(\cosh sx \sin sx - \sinh sx \cos sx) \end{aligned}\right\} \tag{39}$$

The functions $V_i(sx)$,i=1,2,3, obey the following simple rules of differentiation:

$$\left.\begin{aligned} V_0'(sx) &= -s\sqrt{2}\, V_3(sx), \qquad V_1'(sx) = s\sqrt{2}\, V_0(sx) \\ V_2'(sx) &= s\sqrt{2}\, V_1(sx), \qquad V_3'(sx) = s\sqrt{2}\, V_2(sx) \end{aligned}\right\} \tag{40}$$

These rules make the use of these functions of convenience. Introducing the sought solution in the form of Equation 38 into the homogeneous Equation 37, we conclude that the following equation for the factor s of the interfacial peeling stress should be fulfilled:

$$s^8 - (s_1^4 + s_2^4)s^4 + \frac{\delta}{16} = 0 \tag{41}$$

The solution to Equation 41 is given by

$$s = \sqrt[4]{\frac{s_1^4 + s_2^4}{2}\left[1 + \sqrt{1 - \frac{\delta}{4(s_1^4 + s_2^4)^2}}\right]} \tag{42}$$

When the through-thickness interfacial compliance δ_{12} or the compliance δ_{23} is infinitely large (such a situation corresponds to the case of a bi-material assembly), then, as evident from Equation 36, δ = 0. If such a bi-material assembly consists of components 1 and 2, then, in addition to δ = 0, one should also let $\delta_{23} \to \infty$; therefore, following from the second formula in Equations 30, s_2 = 0. Equations 41 and 42 then yield $s = s_1$. Similarly, for a bi-material assembly consisting of components 2 and 3, one obtains $s = s_2$.

Predicted peeling stresses

Using Equations 25 for the shearing stresses, Equations 29 result in the following equations for the interfacial peeling stresses $p_i(x)$, i = 1, 2:

$$\left.\begin{aligned} p_1^{IV}(x) + 4s_1^4 p_1(x) - \frac{p_2(x)}{\delta_{12} D_2} &= -\frac{k^2 h_2}{2\delta_{12} D_2}\left[\left(\frac{h_1}{h_2}\frac{D_2}{D_1} - 1\right)T_1^0 + T_3^0\right]\frac{\cosh kx}{\cosh k\ell} \\ p_2^{IV}(x) + 4s_2^4 p_2(x) - \frac{p_1(x)}{\delta_{23} D_2} &= -\frac{k^2 h_2}{2\delta_{23} D_2}\left[\left(\frac{h_3}{h_2}\frac{D_2}{D_3} - 1\right)T_3^0 + T_1^0\right]\frac{\cosh kx}{\cosh k\ell} \end{aligned}\right\} \tag{43}$$

The particular solutions to these inhomogeneous equations are

$$\bar{p}_1(x) = C_1^* \frac{\cosh kx}{\cosh k\ell}, \qquad \bar{p}_2(x) = C_2^* \frac{\cosh kx}{\cosh k\ell} \tag{44}$$

Introducing these solutions into Equations 43 and solving the resulting equations for the constants C_1^* and C_2^*, we obtain the following formulas for these constants:

$$\left.\begin{aligned} C_1^* &= -\frac{k^2 h_2}{2}\frac{\left[1 + \delta_{23} D_2(k^4 + 4s_2^4)\left(\frac{h_1}{h_2}\frac{D_2}{D_1} - 1\right)\right]T_1^0 + \left[\frac{h_3}{h_2}\frac{D_2}{D_3} - 1 + \delta_{23} D_2(k^4 + 4s_2^4)\right]T_3^0}{\delta_{12}\delta_{23} D_2^2(k^4 + 4s_1^4)(k^4 + 4s_2^4) - 1} \\ C_2^* &= -\frac{k^2 h_2}{2}\frac{\left[1 + \delta_{12} D_2(k^4 + 4s_1^4)\left(\frac{h_3}{h_2}\frac{D_2}{D_3} - 1\right)\right]T_3^0 + \left[\frac{h_1}{h_2}\frac{D_2}{D_1} - 1 + \delta_{12} D_2(k^4 + 4s_1^4)\right]T_1^0}{\delta_{12}\delta_{23} D_2^2(k^4 + 4s_1^4)(k^4 + 4s_2^4) - 1} \end{aligned}\right\} \tag{45}$$

The general solutions to the inhomogeneous Equations 43 can be sought in the form:

$$\left.\begin{aligned} p_1(x) &= A_0' V_0(sx) + A_2' V_2(sx) + C_1^* \frac{\cosh kx}{\cosh k\ell} \\ p_2(x) &= A_0'' V_0(sx) + A_2'' V_2(sx) + C_2^* \frac{\cosh kx}{\cosh k\ell} \end{aligned}\right\} \tag{46}$$

where A'_0, A'_2, A''_0 and A''_2 are the constants of integration. Introducing the solutions given by Equations 46 into the equilibrium conditions of Equations 34, we obtain the following equations for the constants A'_0, A'_2, A''_0 and A''_2 of integration:

$$\left.\begin{aligned} V_1(s\ell)A_0' + V_3(s\ell)A_2' &= -\frac{s\sqrt{2}}{k}C_1^* \tanh k\ell \\ V_2(s\ell)A_0' - [V_0(s\ell) - 1]A_2' &= -\frac{2s^2}{k^2}C_1^* \end{aligned}\right\} \tag{47}$$

and

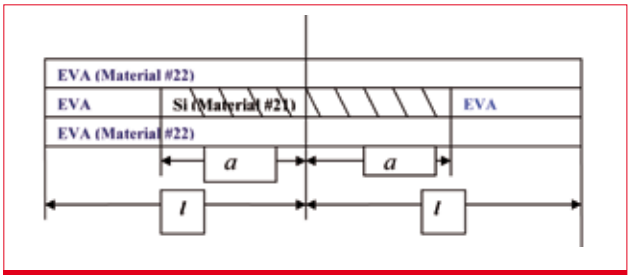

Figure 5. Element of a Si-EVA composite.

$$\left.\begin{aligned} V_1(s\ell)A_0'' + V_3(s\ell)A_2'' &= -\frac{s\sqrt{2}}{k}C_2^* \tanh k\ell \\ V_2(s\ell)A_0'' - [V_0(s\ell)-1]A_2'' &= -\frac{2s^2}{k^2}C_2^* \end{aligned}\right\} \quad (48)$$

The solutions to Equations 47 and 48 are

$$A_0' = -C_1^*\chi_0(s,k),\ A_2' = -C_1^*\chi_2(s,k),\ A_0'' = -C_2^*\chi_0(s,k),\quad A_2'' = -C_2^*\chi_2(s,k) \quad (49)$$

where the functions $\chi_0(s,k)$ and $\chi_2(s,k)$ are expressed as follows:

$$\left.\begin{aligned} \chi_0(s,k) &= \frac{s\sqrt{2}}{k}\ \frac{[V_0(s\ell)-1]\tanh k\ell + \frac{s\sqrt{2}}{k}V_3(s\ell)}{[V_0(s\ell)-1]V_1(s\ell)+V_2(s\ell)V_3(s\ell)} \\ \chi_2(s,k) &= \frac{s\sqrt{2}}{k}\ \frac{V_2(s\ell)\tanh k\ell - \frac{s\sqrt{2}}{k}V_1(s\ell)}{[V_0(s\ell)-1]V_1(s\ell)+V_2(s\ell)V_3(s\ell)} \end{aligned}\right\} \quad (50)$$

Thus, the peeling stresses $p_i(x)$, i = 1, 2, can be evaluated using the formula

$$p_i(x) = -C_i^*\left([\chi_0(s,k)V_0(sx)+\chi_2(s,k)V_2(sx)] - \frac{\cosh kx}{\cosh k\ell}\right),\quad i=1,2 \quad (51)$$

where the constants C_1^* are given by Equations 45.

In the case of a long assembly (large ℓ value) with sufficiently stiff interfaces (large k and s values), the following simplified relationships can be obtained for the functions given by Equations 39:

$$\left.\begin{aligned} V_0(s\ell) &\cong \frac{1}{2}e^{s\ell}\cos s\ell\,, & V_1(s\ell) &\cong \frac{1}{2\sqrt{2}}e^{s\ell}(\sin s\ell + \cos s\ell)\,, \\ V_2(s\ell) &\cong \frac{1}{2}e^{s\ell}\sin s\ell\,, & V_3(s\ell) &\cong \frac{1}{2\sqrt{2}}e^{s\ell}(\sin s\ell - \cos s\ell) \end{aligned}\right\} \quad (52)$$

Equations 50 then yield

$$\left.\begin{aligned} \chi_0(s,k) &= 4\frac{s}{k}e^{-s\ell}\left[\left(1-\frac{s}{k}\right)\cos s\ell + \frac{s}{k}\sin s\ell\right] \\ \chi_2(s,k) &= 4\frac{s}{k}e^{-s\ell}\left[\left(1-\frac{s}{k}\right)\sin s\ell - \frac{s}{k}\cos s\ell\right] \end{aligned}\right\} \quad (53)$$

and solving Equation 51 results in the following simple formula for the distributed peeling stresses:

$$p_i(x) = C_i\left(e^{-k(\ell-x)} - 2\frac{s}{k}e^{-s(\ell-x)}\left[\left(1-\frac{s}{k}\right)\cos(s(\ell-x)) + \frac{s}{k}\sin(s(\ell-x))\right]\right),\quad i=1,2 \quad (54)$$

In the case of $s << k$, Equation 54 yields $p(l) = C_1^*$. Hence, the constants C_1^* expressed by Equations 45 are, in effect, the maximum peeling stresses at the ends of an assembly for which the parameter of the peeling stress s (through-thickness interfacial compliance) is significantly smaller than the shearing stress parameter k (the longitudinal compliance). At the assembly end we have

$$p_i(l) = C_i^*\left(1 - 2\frac{s}{k} + 2\frac{s^2}{k^2}\right),\quad i=1,2 \quad (55)$$

This relationship indicates that, for the given (calculated) C_1^* values, the peeling stresses at the assembly ends are equal to these values for zero $\frac{s}{k}$ ratios of the parameters of the interfacial peeling and shearing stresses, as well as for the situation when this ratio is equal to one. Equation 55 also indicates that the peeling stresses at the assembly ends have a minimum of for the stress parameter

Property	Thickness h [mm]	Young's Modulus E, [kg/mm^2]***	Poisson's Ratio ν	2D Young's Modulus $E^* = \frac{E}{1-\nu}$, [kg/mm^2]	Shear Modulus $G = \frac{E}{2(1+\nu)}$, *** [kg/mm^2]	CTE $\alpha x 10^6$ [1/°C]
# Material			Input data			
1 Glass	5.00	7150	0.22	9167	2930	5.0
21 Silicon	0.20	16000	0.28	22222	6250	2.6
22 EVA 0.30	100	0.35	154	100	100	
2 Si-EVA Composite*	0.50	5506	0.326	8169	2076	42.5
3 Backsheet**	0.25	300	0.40	500	107	33

* Properties were evaluated for a segment of the Si-EVA composite structure (Fig. 2) using the formulas

$$E_{2e} = \frac{a}{l}\left(\frac{E_{21}h_{21} + E_{22}h_{22}}{h_{21}+h_{22}} - E_{22}\right) + E_{22} = \frac{0.34}{0.4}\left(\frac{16000x0.2 + 100x0.3}{0.2+0.3} - 100\right) + 100 = 5506kg/mm^2$$

$$\nu_{2e} = \frac{a}{l}\left(\frac{\nu_{21}h_{21} + \nu_{22}h_{22}}{h_{21}+h_{22}} - \nu_{22}\right) + \nu_{22} = \frac{0.34}{0.4}\left(\frac{0.28x0.2 + 0.35x0.3}{0.2+0.3} - 0.35\right) + 0.35 = 0.326$$

$$\alpha_{2e} = \frac{a}{l}\left(\frac{\alpha_{21}E_{21}h_{21} + \alpha_{22}E_{22}h_{22}}{E_{21}h_{21} + E_{22}h_{22}} - \alpha_{22}\right) + \alpha_{22} =$$

$$= \left[\frac{0.34}{0.40}\left(\frac{2.6x16000x0.2 + 100x100x0.3}{1600x0.2 + 100x0.3} - 100\right) + 100\right]x10^{-6} = 42.5x10^{-6}1/^0C$$

In these formulas it is assumed that the length of the Si-EVA segment is $2l$=0.80mm, the length of the Si cell in it is $2a$=0.68mm, the cell thickness is h_{21}=0.20mm, the total thickness of the Si-EVA composite is $h_{21}+h_{22}$=0.50mm, and the thickness of the EVA above the Si cell is the same as below it and equal to 0.15mm.

** Polyethylene terephthalate (PET) polyester

*** For details see http://www.americanelements.com/thermal-expansion-coe.html or http://www1.eere.energy.gov/solar/pdfs/pvmrw2011_p41_csi_ebert.pdf. The change in temperature from the EVA curing temperature of 158°C to the room temperature is assumed to be Δt = 30°C.

Table 1. Material properties of the PVM for the numerical example.

ratio of 0.5, and that the peeling stresses can be very high for high stress parameter ratios.

Stresses in the composite EVA-Si layer

The problem

The objective of the following analysis is to address the state of stress within the EVA-Si composite layer (Fig. 5). In addition to the thermal contraction mismatch forces due to the dissimilar Si and EVA materials, the layer is subjected to an external tensile force $\hat{T} = T_2^0$. This force is determined on the basis of the previous analysis, when the effective mechanical characteristics of the Si-EVA composite were considered. In the following analysis, the actual properties of the EVA and Si materials are taken into account, in addition to the geometric characteristics of the Si cells (length and thickness) and the thickness of the EVA encapsulant. The analysis is limited to the evaluation of the normal stresses acting in the cross sections of the Si cells and the EVA materials, and the interfacial shearing stresses that are responsible for the possible delamination of the EVA encapsulant from the Si cells.

Basic equation

The induced axial forces $T_{21}(x)$ and $T_{21}(x)$, acting in the Si device (material 2-1) embedded into the EVA encapsulant and acting in the encapsulant itself (material 2-2), respectively, and caused by the combined action of the thermal and mechanical loading on component 2 of the PV assembly, are related as follows:

$$T_{21}(x) + T_{22}(x) = \hat{T}, \quad T_{21}(x) = 2\int_{-a}^{x}\tau(\xi)d\xi, \quad T_{22}(x) = \hat{T} - 2\int_{-a}^{x}\tau(\xi)d\xi \qquad (56)$$

The origin of the coordinate x is in the mid-cross section of the Si cell. In Equations 56, $\tau(x)$ is the interfacial shearing stress and a is half the Si cell length. Since the upper and the lower parts (layers) of the EVA encapsulant are assumed to be identical, it follows that 1) the stress $\tau(x)$ is the same at the upper and lower Si-EVA interfaces, and 2) the assembly as a whole does not experience bending deformations. Clearly, $\int_{-a}^{a}\tau(\xi)d\xi = 0$ (the shearing stress is anti-symmetric with respect to the mid-cross section of the Si cell). As evident from Equations 56, the boundary conditions $T_{21}(\pm a) = 0$ (this condition is based on our assumption that no external forces are applied directly to the butt end of the Si cell) and $T_{22}(\pm a) = \hat{T}$ are fulfilled for the forces $T_{21}(x)$ and $T_{22}(x)$. From Equations 56 we find, by differentiation,

$$\tau(x) = \frac{1}{2}T'_{21}(x) = -\frac{1}{2}T'_{22}(x) \qquad (57)$$

We seek the longitudinal interfacial displacements of the Si cell and the EVA encapsulant as follows:

$$u_1(x) = -\alpha_{21}\Delta t x + \lambda_{21}\int_0^x T_{21}(\xi)d\xi - 2\kappa_{21}\tau(\xi),$$
$$u_2(x) = -\alpha_{22}\Delta t x + \lambda_{22}\int_0^x T_{22}(\xi)d\xi + 2\kappa_{22}\tau(\xi) \qquad (58)$$

where a_{21} and a_{22} are the CTEs of the Si cell and the EVA materials, respectively; Δt is the change in temperature; $\lambda_{21}=\frac{1-\nu_{21}}{E_{21}h_{21}}$ and $\lambda_{22}=\frac{1-\nu_{22}}{2E_{22}h_{22}}$ are the axial compliances of the cell and the encapsulant; h_{21} is the cell thickness; h_{22} is the thickness of the encapsulant above or beneath the die; E_{21} and E_{22} are the Young's moduli of the Si and the EVA materials; and ν_{21} and ν_{22} are their Poisson's ratios. Also,

$$\kappa_{21}=\frac{h_{21}}{6G_{21}},\ \kappa_{22}=\frac{h_{22}}{3G_{22}}, \tag{59}$$

are the interfacial shearing compliances of the Si cell and each of the EVA layers (above and below the cell), respectively, and $G_{21}=\frac{E_{21}}{2(1+\nu_{21})}$ and $G_{22}=\frac{E_{22}}{2(1+\nu_{22})}$ are the shear moduli of the materials. The first of Equations 59 was obtained in Suhir [18] for a strip subjected to a shear load distributed over both of its long edges and symmetric with respect to its mid-cross section and to the horizontal mid-plane of the strip. The second of Equations 59 was obtained in Suhir [17] for a strip subjected to a shear load distributed over one of its long edges and symmetric with respect to the mid-cross section of the component.

The condition of the compatibility of the displacements given by Equations 58 can be written as

$$u_1(x)=u_2(x)+\kappa_0\tau(x) \tag{60}$$

where $\kappa_0=\frac{h_0}{G_0}$ is the interfacial compliance of an additional layer, if any, between the Si cell and the encapsulant, h_0 is its thickness and G_0 is the shear modulus of the material. Introducing Equations 58 into the compatibility condition of Equation 60, we obtain the following basic equation for the interfacial shearing stress $\tau(x)$:

$$\tau(x)-\frac{\lambda_{21}}{2\kappa}\int_0^x T_{21}(\xi)d\xi+\frac{\lambda_{22}}{2\kappa}\int_0^x T_{22}(\xi)d\xi=\frac{\varepsilon_t}{2\kappa}x, \tag{61}$$

where $\varepsilon_t=\Delta\alpha\Delta t=(\alpha_{22}-\alpha_{21})\Delta t$ is the thermal mismatch strain and $\kappa=\kappa_0+\kappa_{21}+\kappa_{22}$ is the total interfacial compliance of the assembly. The integrands in Equation 61 are related to the interfacial shearing stress $\tau(x)$ by the formulas expressed by Equations 56.

From Equation 61 we obtain, by differentiation,

$$\tau'(x)-\frac{\lambda_{21}}{2\kappa}T_{21}(x)+\frac{\lambda_{22}}{2\kappa}T_{22}(x)=\frac{\varepsilon_t}{2\kappa} \tag{62}$$

This relationship allows the boundary conditions $T_{21}(\pm a)=0$ and $T_{22}(\pm a)=\hat{T}$ for the forces to be translated into the boundary condition for the shearing stress function $\tau(x)$ as follows:

$$\tau'(a)=-\frac{\lambda_{22}}{2\kappa}\hat{T}+\frac{\varepsilon_t}{2\kappa} \tag{63}$$

Differentiating Equation 62 with respect to the coordinate x yields the following simple equation for the interfacial shearing stress function $\tau(x)$:

$$\tau''(x)-k^2\tau(x)=0 \tag{64}$$

where $k=\sqrt{\frac{\lambda}{\kappa}}$ is the parameter of the interfacial shearing stress, and $\lambda=\lambda_{21}+\lambda_{22}$ is the total axial compliance of the Si-EVA assembly.

Solution to the basic equation

Equation 64 has the following solution that satisfies the boundary condition of Equation 63:

$$\tau(x)=-\frac{1}{2}kT\frac{\sinh kx}{\cosh ka} \tag{65}$$

where $T=T_m-T_t$ is the force acting in the mid-portion of a Si-EVA assembly with a sufficiently long cell (large a values) and/or with a sufficiently stiff interface (large k values); $T_m=\frac{\lambda_{22}}{\lambda}\hat{T}$ is the tensile force due to the 'external' tensile force; $\hat{T}$ and $T_t=\frac{\varepsilon_t}{\lambda}=\frac{\Delta\alpha\Delta t}{\lambda}$ is the compressive force in the Si cell caused by the thermal contraction mismatch of the Si and the EVA materials.

The reduction factor $\frac{\lambda_{22}}{\lambda}=\frac{1}{1+\frac{\lambda_{21}}{\lambda_{22}}}$ in front of the force $\hat{T}$ is the ratio of the axial compliance of the EVA layer to the total axial compliance of the Si-EVA assembly. When the encapsulant is significantly more compliant than the Si cell ($\lambda_2 \triangleright\triangleright \lambda_1$), the ratio $\frac{\lambda_{22}}{\lambda}$ is close to 1, so that the entire external force $\hat{T}$ is transmitted to the Si device. In this case the encapsulant exhibits tensile thermal loading only, i.e. $T_t=\frac{\varepsilon_t}{\lambda_{22}}=2\frac{E_{22}}{1-\nu_{22}}h_{22}\varepsilon_t$. In the hypothetical situation of the encapsulant layer being appreciably less compliant than the Si cell ($\lambda_{22} \triangleleft\triangleleft \lambda_{21}$) – which is certainly not the case for the design in question – the ratio $\frac{\lambda_{22}}{\lambda}$ becomes $\frac{\lambda_{22}}{\lambda_{21}}$. This ratio is close to zero when the EVA encapsulant is significantly less compliant than the Si cell. The Si cell consequently becomes stress free, and it is the encapsulant that experiences the full magnitude of the force $\hat{T}$.

In the case of sufficiently large and/or stiff Si-EVA assemblies ($ka \geq 2.5$), the solution given by Equation 65 can be simplified to $\tau(x)=-\frac{1}{2}kTe^{-k(a-x)}$. This formula indicates that the shearing stress at the Si-EVA interface concentrates at the Si-EVA assembly ends, and decreases exponentially with increasing distance from the ends. In the hypothetical case of a small and/or compliant Si-EVA assembly ($ka \leq 0.25$), the solution (Equation 65) can be simplified to $\tau(x)=-\frac{1}{2}k^2Tx$. In this case the stress is distributed linearly along the Si-EVA interface. As follows from Equation 65, the maximum shearing stress τ_{max} takes place at the end cross sections $x=\pm a$ and is given by $x=\pm a:\ \tau_{max}=\tau_{max}^{\infty}\chi_\tau(ka)$, where $\tau_{max}^{\infty}=-\frac{1}{2}kT$ is the maximum interfacial shearing stress in an infinitely long assembly, and the function $\chi_\tau(ka)=\tanh ka$ accounts for the effect of the assembly size.

Introducing the solution (Equation 65) into the formulas (Equations 56), we obtain

$$T_{21}(x)=T\left(1-\frac{\cosh kx}{\cosh ka}\right),\ T_{22}(x)=\hat{T}-T\left(1-\frac{\cosh kx}{\cosh ka}\right)=T\left(\frac{\lambda_{21}}{\lambda_{22}}+\frac{\cosh kx}{\cosh ka}\right)+T_t\frac{\lambda}{\lambda_{22}} \tag{66}$$

The force $T_{21}(x)$ acting in the Si cell is greatest in its mid-cross section ($x=0$) and is given by $T_{21}(0)=T\chi_\sigma(ka)$, where the function $\chi_\sigma(ka)=\frac{T_{21}(0)}{T}=1-\frac{1}{\cosh ka}$ takes into account the effect of the Si-EVA assembly size. For sufficiently long assemblies (large a) and/or assemblies with stiff interfaces (large k), so that $ka \geq 2.5$, we have $T_{21}(0)=T$ For a short (small a) and/or compliant (small k) Si-EVA assembly ($ka \leq 0.25$), the first of Equations 66 yields $T_{21}(x)=T_{21}(0)\left(1-\frac{x^2}{a^2}\right)$, where $T_{21}(0)=T\frac{(ka)^2}{2}$ is the force in the mid-cross section of the device. The corresponding normal stress can be found by dividing the force $T_{21}(x)$ by the Si cell thickness h_{21}. If the product ka is small, then the force $T_{21}(0)$ is small as well. Thus, for lower induced stresses in the cwell, there is an incentive to employ, if possible, small-sized cells and compliant bonding layers, if any, between the Si and the EVA materials.

Numerical example

Fig. 2 shows the structure under consideration, and its material characteristics (input data) are given in Table 1. The calculations are set forth below.

Axial compliances of the assembly components

$$\lambda_1 = \frac{1}{E_1^* h_1} = \frac{1}{9167x5.0} = 2.1817x10^{-5}\, mm/kg,$$
$$\lambda_2 = \frac{1}{E_2^* h_2} = \frac{1}{8169x0.5} = 24.4828x10^{-5}\, mm/kg,$$
$$\lambda_3 = \frac{1}{E_3^* h_3} = \frac{1}{500x0.25} = 8.0000x10^{-5}\, mm/kg,$$

Flexural rigidities of the assembly components

$$D_1 = \frac{E_1 h_1^3}{12(1-\nu_1^2)} = \frac{7150x5.0^3}{12(1-0.22^2)} = 78267.3042 kgmm$$
$$D_2 = \frac{E_2 h_2^3}{12(1-\nu_2^2)} = \frac{5506x0.5^3}{12(1-0.326^2)} = 64.1744 kgmm$$
$$D_3 = \frac{E_3 h_3^3}{12(1-\nu_3^2)} = \frac{300x0.25^3}{12(1-0.4^2)} = 0.4650 kgmm$$
$$D = D_1 + D_2 + D_3 = 78331.9436 kgmm$$

Combined axial compliances of the assembly components

$$\lambda_{11} = \frac{(h_1+h_2)^2}{4D} + \lambda_1 + \lambda_2 = \frac{(5.0+0.5)^2}{4x78331.9436} + 2.1817x10^{-5} + 24.4828x10^{-5} =$$
$$= 36.3189x10^{-5}\, mm/kg$$
$$\lambda_{33} = \frac{(h_2+h_3)^2}{4D} + \lambda_2 + \lambda_3 = \frac{(0.5+0.25)^2}{4x78331.9436} + 24.4828x10^{-5} + 8.0000x10^{-5} =$$
$$= 32.6623x10^{-5}\, mm/kg$$
$$\lambda_{13} = \frac{(h_1+h_2)(h_2+h_3)}{4D} - \lambda_2 = \frac{(5.0+0.5)(0.5+0.25)}{4x78331.9436} - 24.4828x10^{-5} =$$
$$= -23.1663x10^{-5}\, mm/kg$$

Interfacial compliances

$$\kappa_1 = \frac{h_1}{3G_1} = \frac{5.00}{3x2930} = 56.8828x10^{-5}\, mm^3/kg,$$
$$\kappa_2 = \frac{h_2}{G_2} = \frac{0.5}{2076} = 24.0848x10^{-5}\, mm^3/kg,$$
$$\kappa_3 = \frac{h_3}{3G_3} = \frac{0.25}{3x107} = 77.8816x10^{-5}\, mm^3/kg,$$

Combined (coupled) interfacial compliances

$$\kappa_{12} = \kappa_1 + \kappa_2 = 80.9676x10^{-5}\, mm^3/kg,\ \kappa_{23} = \kappa_2 + \kappa_3 = 101.9664x10^{-5}\, mm^3/kg,$$

Parameter of the interfacial shearing stresses

$$k_1 = \sqrt{\frac{\lambda_{11}}{\kappa_{12}}} = \sqrt{\frac{36.3189x10^{-5}}{80.9676x10^{-5}}} = 0.6697 mm^{-1};\ k_2 = \sqrt{\frac{\lambda_{33}}{\kappa_{23}}} = \sqrt{\frac{32.6623x10^{-5}}{101.9664x10^{-5}}} = 0.5660 mm^{-1};$$
$$\gamma = 1 - \frac{\lambda_{13}^2}{\lambda_{11}\lambda_{33}} = 1 - \frac{(-23.1663x10^{-5})^2}{36.3189x10^{-5}x32.6623x10^{-5}} = 0.5476,$$
$$k = \sqrt{\frac{k_1^2+k_2^2}{2}\left[1+\sqrt{1-\gamma\left(\frac{2k_1k_2}{k_1^2+k_2^2}\right)^2}\right]} = \sqrt{\frac{0.7689}{2}\left[1+\sqrt{1-0.5476\left(\frac{0.7581}{0.7689}\right)^2}\right]} = 0.8046 mm^{-1}$$

Thermally induced forces acting in the cross sections of the assembly components

$$T_1^0 = \frac{\lambda_2(\alpha_1-\alpha_3)+\lambda_3(\alpha_1-\alpha_2)}{\lambda_1\lambda_2+\lambda_2\lambda_3+\lambda_3\lambda_1}\Delta t =$$
$$= \frac{24.4828\ x10^{-5}(5.0-33.0)x10^{-6} + 8.0000\ x10^{-5}(5.0-42.5)x10^{-6}}{2.1817\ x10^{-5}x24.4828\ x10^{-5} + 24.4828\ x10^{-5}x8.0000\ x10^{-5} + 8.0000\ x10^{-5}x2.1817\ x10^{-5}}130 =$$
$$= \frac{-685.5184\ x10^{-11} - 300.0000\ x10^{-11}}{53.4141\ x10^{-10} + 195.8624\ x10^{-10} + 17.4536\ x10^{-10}}130 = -\frac{985.5184\ x10^{-11}}{266.7301\ x10^{-10}}130 = -48.0326\ kg/mm$$

$$T_2^0 = \frac{\lambda_3(\alpha_2-\alpha_1)+\lambda_1(\alpha_2-\alpha_3)}{\lambda_1\lambda_2+\lambda_2\lambda_3+\lambda_3\lambda_1}\Delta t = \frac{8.0000x10^{-5}x(42.5-5.0)x10^{-6} + 2.1817x10^{-5}(42.5-33)x10^{-6}}{266.7301x10^{-10}}130 =$$
$$= \frac{300.0000x10^{-11} + 20.7262x10^{-11}}{266.7301x10^{-10}}130 = 15.6317\ kg/mm$$

$$T_3^0 = \frac{\lambda_1(\alpha_3-\alpha_2)+\lambda_2(\alpha_3-\alpha_1)}{\lambda_1\lambda_2+\lambda_2\lambda_3+\lambda_3\lambda_1}\Delta t = \frac{2.1817\ x10^{-5}(33-42.5)x10^{-6} + 24.4828\ x10^{-5}(33-5)x10^{-6}}{266.7301\ x10^{-10}}130 =$$
$$= \frac{-20.7262\ x10^{-11} + 685.5184\ x10^{-11}}{266.7301\ x10^{-10}}130 = 32.4009\ kg/mm$$

Normal stresses in the mid-portions of the glass and the backsheet

$$\sigma_1^0 = \frac{T_1^0}{h_1} = -\frac{48.0326}{5.0} = -9.6065 kg/mm^2$$

$$\sigma_3^0 = \frac{T_3^0}{h_3} = \frac{32.4009}{0.25} = 129.6036 kg/mm^2$$

Stress in the EVA material outside the Si cell

$$\sigma_2^0 = \frac{T_2^0}{h_2} = \frac{15.6317}{0.5} = 31.2634 kg/mm^2$$

Axial compliance of the Si-EVA layer

$$\lambda = \frac{1}{E_{21}^* h_{21}} + \frac{1}{E_{22}^* h_{22}} = \frac{1}{22222x0.2} + \frac{1}{154x0.3} = 22.5002x10^{-5} + 2164.5022x10^{-5} =$$
$$= 2187.0022x10^{-5}\, mm/kg$$

Interfacial compliance of the Si-EVA layer

$$\kappa = \frac{h_{21}}{6G_{21}} + \frac{2h_{22}}{3G_{22}} = \frac{0.2}{6x6250} + \frac{2x0.15}{3x100} = 0.5333x10^{-5} + 100x10^{-5} = 100.5333x10^{-5}\, mm^3/kg$$

Parameter of the interfacial shearing stress for the Si-EVA composite

$$k_{Si} = \sqrt{\frac{\lambda}{\kappa}} = \sqrt{\frac{2192.1954x10^{-5}}{100.5333x10^{-5}}} = 4.6697$$

Factor for considering the effect of the finite size of the Si cell on the induced thermal force

$$\chi_\sigma(k_{Si}a) = 1 - \frac{1}{\cosh k_{Si}a} = 1 - \frac{1}{\cosh(4.6697x0.34)} = 0.6076$$

'Mechanical' tensile forces acting on the EVA and Si material within the area where Si cells are located

$$T_{22}^0 = \frac{E_{22}h_{22}T_2^0}{E_{21}h_{21}+E_{22}h_{22}}\chi_\sigma(k_{Si}a) = \frac{100x0.3x15.6317}{16000x0.2+100x0.3}0.6076 = 0.0882 kg/mm$$
$$T_{21}^0 = \frac{E_{21}h_{21}T_2^0}{E_{21}h_{21}+E_{22}h_{22}}\chi_\sigma(k_{Si}a) = \frac{16000x0.2x15.6317}{16000x0.2+100x0.3}0.6076 = 9.4096 kg/mm$$

Thermally induced force in the EVA-Si composite within the area where Si cells are located

$$T_t = \frac{\Delta\alpha\Delta t}{\lambda}\chi_\sigma(k_{Si}a) = \frac{(100-2.6)x10^{-6}x130}{2192.1954x10^{-5}}0.6076 = 0.3509 kg/mm$$

Tensile force in the EVA layer due to the combined action of the external ('mechanical') and thermal loading

$$T_{EVA} = T_{22}^0 + T_t = 0.0882 + 0.3509 = 0.4391 kg/mm$$

Normal stress in the EVA layer

$$\sigma_{EVA} = \frac{T_{EVA}}{h_{22}} = \frac{0.4391}{0.3} = 1.4638 kg/mm^2$$

Tensile force in the Si layer within the area where Si cells are located

$$T_{Si} = T_{21}^0 - T_t = 9.4096 - 0.3509 = 9.0587 kg/mm$$

Normal stress in the Si cell within the area where Si cells are located

$$\sigma_{Si} = \frac{T_{Si}}{h_{21}} = \frac{9.0587}{0.2} = 45.2935 kg/mm^2$$

Maximum shearing stress at the Si-EVA interface

$$\tau_{\max} = k_{Si} T_{Si} \tanh ka = 4.6697x9.0587x \tanh(4.6697x0.34) = 38.9078 kg/mm^2$$

Maximum shearing stress at the glass-EVA interface

$$\tau_{1,\max} = -kT_1^0 = 0.8171x\ 107.0499 = 87.4705 kg/mm^2$$

Maximum shearing stress at the EVA-backsheet interface

$$\tau_{2,\max} = -kT_3^0 = -0.8171x\ 22.3519 = -18.2637 kg/mm^2$$

Compliances in the through-thickness direction

$$\delta_{12} = \frac{h_1}{E_1^*} + \frac{h_2}{2E_2^*} = \frac{5.0}{9167} + \frac{0.5}{2x154} = 0.00054543 + 0.00162338 = 0.0021688 mm^3/kg$$

$$\delta_{23} = \frac{h_3}{E_3^*} + \frac{h_2}{2E_2^*} = \frac{0.25}{500} + \frac{0.5}{2x154} = 0.000500 + 0.00162338 = 0.0021234 mm^3/kg$$

$$s_1 = \sqrt[4]{\frac{D_1 + D_2}{4\delta_{12} D_1 D_2}} = \sqrt[4]{\frac{78267.3042 + 64.1744}{4x0.0021688x78267.3042x64.1744}} = 1.1579 mm^{-1}$$

$$s_2 = \sqrt[4]{\frac{D_2 + D_3}{4\delta_{23} D_2 D_3}} = \sqrt[4]{\frac{64.1744 + 0.4650}{4x0.0021234x64.1744x0.4650}} = 3.9962 mm^{-1}$$

$$\delta = \frac{D}{\delta_{12}\delta_{23} D_1 D_2 D_3} = \frac{78331.9436}{0.0021688x0.0021234x78267.3042x64.1744x0.4650} = 7282.7003 mm^{-8}$$

Parameter of the peeling stresses

$$s = \sqrt[4]{\frac{s_1^4 + s_2^4}{2}\left[1 + \sqrt{1 - \frac{\delta}{4(s_1^4 + s_2^4)^2}}\right]} = \sqrt[4]{\frac{1.7976 + 255.0286}{2}\left[1 + \sqrt{1 - \frac{7282.7003}{4x256.8262^2}}\right]} = 3.9963 mm^{-1}$$

Constants in the expression for the peeling stress functions

$$C_1^* = -\frac{k^2 h_2}{2} \frac{\left[1 + \delta_{23} D_2 (k^4 + 4s_2^4)\left(\frac{h_1}{h_2}\frac{D_2}{D_1} - 1\right)\right] T_1^0 + \left[\frac{h_3}{h_2}\frac{D_2}{D_3} - 1 + \delta_{23} D_2 (k^4 + 4s_2^4)\right] T_3^0}{\delta_{12}\delta_{23} D_2^2 (k^4 + 4s_1^4)(k^4 + 4s_2^4) - 1} =$$

$$= -0.1618 \frac{6576.8937 + 6709.2759}{146.2830} = -14.6955 kg/mm^2$$

$$C_2^* = -\frac{k^2 h_2}{2} \frac{\left[1 + \delta_{12} D_2 (k^4 + 4s_1^4)\left(\frac{h_3}{h_2}\frac{D_2}{D_3} - 1\right)\right] T_3^0 + \left[\frac{h_1}{h_2}\frac{D_2}{D_1} - 1 + \delta_{12} D_2 (k^4 + 4s_1^4)\right] T_1^0}{\delta_{12}\delta_{23} D_2^2 (k^4 + 4s_1^4)(k^4 + 4s_2^4) - 1} =$$

$$= -0.1618 \frac{2366.0080 - 3.2320}{146.2830} = -2.6134 kg/mm^2$$

Ratio of the peeling stress parameter to the shearing stress parameter

$$\frac{s}{k} = \frac{3.9963}{0.8046} = 4.9668$$

Maximum peeling stresses

$$p_1(l) = C_1\left(1 - 2\frac{s}{k} + 2\frac{s^2}{k^2}\right) = -14.6955x40.4046 = -593.7659 kg/mm^2$$

$$p_2(l) = C_2\left(1 - 2\frac{s}{k} + 2\frac{s^2}{k^2}\right) = -2.6134x40.4046 = -105.5934 kg/mm^2$$

The calculated stresses are summarized in Table 2. The computed data indicate that the interfacial peeling stresses considerably exceed the interfacial shearing stresses and could possibly lead, in combination with the effect of the shearing stresses, to delaminations. These data also indicate that delaminations at the glass-encapsulant interface are more likely than delaminations at the backsheet-encapsulant interface. As for the stresses acting in the components' cross sections, these are greatest in the backsheet, and need to be taken into consideration when the material and the thickness of the backsheet are selected and established.

Material (layer)	Stress in the component cross section [kg/mm²]	Maximum interfacial stresses [kg/mm²]	
		Shearing	Peeling
Glass	–9.6		
Glass-EVA Interface		87.5	593.7
EVA	+31.3		
EVA-Si Interface		38.9	-
Si	+45.3		
Si-EVA Interface		38.9	-
EVA	+31.3		
EVA-Backsheet Interface		18.3	105.6
Backsheet	+129.6		

Table 2. Calculated stresses for the numerical example.

> "Important as the reliability and performance of a PV device itself is, it is the module – or the 'package' – that is the most vulnerable element of a PVM."

Some major challenges and future work

Since solar energy is abundant worldwide, cell/PV technology is an attractive option in the renewable energy field, but there is still a long way to go before viable and promising devices based on PV technology become reliable and cost-effective products. Here are a few of the main questions that are typically asked and some of the major challenges envisioned:

- Since some (far from perfect) PV products have been in the field for just a couple of years, no well-established qualification specifications and test methodologies exist yet. For this reason, the only way to make adequate short- and long-term reliability predictions, as far as the possible failure modes and mechanisms are concerned, is through properly designed, carefully conducted and clearly interpreted failure-oriented accelerated testing (FOAT). What stimuli and reliability criteria should be included in such FOAT methodologies and testing procedures? Should we be aiming (perhaps unrealistically) for a 20-year PVM lifetime, or possibly settle for a shorter lifetime?

- How will actual loading (thermal, dynamic) and environmental (temperature, humidity, earthquake, etc.) conditions

encountered in different geographic areas affect the useful and cost-effective lifetime of the PV system of interest, and what should be the criteria?

- The major effort today centres on improving the effectiveness and reliability of PV devices per se. However, it is clear that, important as the reliability and performance of a PV device itself is, it is the module – or the 'package' – that is the most vulnerable element of a PVM. Should the PVM engineering and business-oriented communities, concurrently with the continuing effort to make the PV devices more efficient and more robust, place more emphasis on the general reliability of PVM systems (structures)? Are the existing PV qualification test methodologies and procedures – such as IEC 61215 (for crystalline-Si-based devices), IEC 61646 (for thin-film-based devices) and IEC 62108 (for concentration-based devices (CPV)) – adequate? Do PV industries need new approaches to qualify their products?

- The most critical aspect of today's PV technologies seems to be the way(s) in which a PVM is packaged (optical, electrical, materials, thermo-mechanical, etc.) to protect the given PVM design from the harsh environment, in order to enhance what the PV devices can do and to guarantee, with a reasonably high certainty, their durability. There is a crucial need to consider and to develop effective and goal-oriented PVM packaging directions – what is the best way to do this and how can it be done in a timely fashion? To what extent could previous experience, accumulated in the fields of electronics, opto-electronics, photonics, MEMS and MOEMS technologies, be employed?

- In many areas of opto-electronic engineering, predictive modelling has proved to be a highly useful and time-effective means of both understanding the physics of failure and designing the most helpful FOAT. There is certainly a need for developing such models in the PV field, with an emphasis on validating observed field failures. Which models might be needed most: thermal, environmental or mechanical – or combinations of all these?

- There are indications that some PVM degradation (ageing) and failure mechanisms have been found in the field that were not detected by the existing accelerated tests, such as temperature cycling, temperature-humidity bias (THB), nominal operating cell temperature (NOCT), hail (solid precipitation) tests and high-voltage (high-potential, or 'high-pot') tests. How can a minimum list of crucial tests and stimuli be established?

- There are currently several different PV technologies (key approaches to solar-based electricity), such as solar thermal, crystalline Si, thin film, concentrators and, perhaps, combinations of these. Each of these technologies has its merits and shortcomings. Should the packaging and FOAT approaches be developed separately for all these technologies, or might there be unified and cost- and time-effective ways of addressing reliability and packaging issues for them? Is there a possibility that one or two existing PV technologies will predominate (or perhaps already do so), and that packaging and reliability efforts should be directed accordingly?

- There are many PVM reliability concerns that are more or less well established – some examples are:
  - if new materials and/or new physical (structural) designs are introduced, how will this affect the short- and long-term reliability of the PV device and/or the PVM and/or the PVM system as a whole?
  - to what extent could impurities in the silicon result in light-induced degradation of the material?
  - how might arcing, grounding, power conditioning and other system-related problems affect the PV system's reliability?
  - given that annual degradation rates of typically 0–1% might be difficult to measure, how could one measure, using existing metrological techniques, even lower degradation rates (less than 0.1%) in the field? Could better metrological means be developed, and what role might modelling play in such a situation?
  - edge seals in the moisture-resistant device structures may allow water penetration; at the same time it has been established that thermal stresses due to dissimilar materials concentrate at the assembly ends. How could this thermo-mechanical-environmental problem, as well as many other adhesion-related problems, be resolved?

- The process involved in going from creating something in a lab to marketing an industrial product is a lengthy one. Could this be shortened?

- The measurement of degradation rates takes several years. Could physically meaningful ALT (accelerated-life test)-FOAT methodologies be developed?

Based on the authors' expertise in many areas of reliability and packaging of electronic systems, a list is presented below of the most crucial engineering problems that could be addressed and successfully solved, and that are, at the same time, of the utmost interest to the PV manufacturing community.

- Review and analyze existing PVM physical designs and the geographical areas in which these modules are, or will be, installed.

- Review and analyze the existing qualification testing specifications and test conditions used by Flextronics to qualify its PVM systems.

- Review and analyze any observed field failures of the PV products.

- Address the adequacy of the existing Flextronics specifications and accelerated test methodologies and practices from the standpoint of their ability to prevent field failures.

- Improve in a timely fashion and to the extent possible the existing qualification methodologies.

- Select the most indicative and most vulnerable structural item (the 'bottle-neck') in the existing Flextronics PVM design, and then consider the application to the selected structural element of the recently suggested (rather general) novel and effective approach [18–20] for qualifying electronic and similar products.

- Design an adequate FOAT procedure, conduct the accelerated life testing, develop the appropriate predictive models and predict the reliability of failure of the selected structural element in the field.

- On the basis of the results obtained, make a prediction, using primarily predictive modelling approaches and techniques (both computer-aided and analytical), of the probability of failure of the entire PVM system in the field under the anticipating loading conditions and after the given time in operation.

- Establish what changes, if any, to the existing design and in the qualification specifications could or should be made.

Experimental and modelling (both computer-aided and analytical) approaches should and will be widely used to address these issues.

"The model can also be used for stress analysis and reliability predictions for bonded joints in applications outside of the PV technology field."

Conclusions

Low-temperature thermally induced stresses in a crystalline-Si-based PVM (assembly) have been evaluated on the basis of a rather general analytical ('mathematical') predictive stress model for a tri-material assembly. A special predictive model was developed for the evaluation of the effective elastic constants and the CTE of component 2 (EVA-Si composite) consisting of a low-modulus and high-expansion EVA encapsulant and high-modulus and low-expansion Si cells, so that the module of interest could be treated as a tri-material body. The calculated data indicated that the induced stresses can be rather high, especially the peeling stress at the glass interface, which means that the structural integrity of the PVM might be compromised unless the appropriate DfR measures are taken. It is well known that the reliability of a product should be conceived and, to the extent possible, assured at the design stage – as far as such an effort is concerned, the developed model can be helpful. The model can also be used for stress analysis and reliability predictions for bonded joints in applications outside of the PV technology field.

References

[1] Meydbray, J. et al. 2007, "Solder joint degradation in high efficiency all back contact solar cells", *Proc. 22nd EU PVSEC*, Milan, Italy.

[2] Osterwald, C. & McMahon, T. 2008, "History of accelerated and qualification testing of terrestrial photovoltaic modules: A literature review", *Prog. Photovolt: Res. Appl.*, Vol. 17.

[3] Wohlgemuth, J.H. et al. 2008, "Using accelerated tests and field data to predict module reliability and lifetime", *Proc. 23rd EU PVSEC*, Valencia, Spain.

[4] Jacobson, M.Z. 2008, "Review of solutions to global warming, air pollution, and energy security", The Energy Seminar, Stanford University, October 1 [available online at http://www.stanford.edu/group/efmh/jacobson/Articles/I/ReviewSolGW09.pdf].

[5] Hacke, P. et al. 2010, "Test-to-failure of crystalline silicon modules", *Proc. 35th IEEE PVSC*, Honolulu, Hawaii, USA.

[6] Dietrich, S. et al. 2010, "Mechanical and thermo-mechanical assessment of encapsulated solar cells by finite-element-simulation", *Proc. SPIE - Optics and Photonics*, San Diego, California, USA.

[7] Meier, R. et al. 2010, "Thermal and mechanical induced loading on cell interconnectors in crystalline photovoltaic modules", *Proc. 25th EU PVSEC*, Valencia, Spain.

[8] Schubbert, C. et al. 2010, "Exemplary results of temperature-dependent mechanical load tests under variation of glass and foil parameters and investigation of different load types", *Proc. 25th EU PVSEC*, Valencia, Spain.

[9] Lau, J.H. (Ed.) 1993, *Thermal Stress and Strain in Microelectronics Packaging*. New York: Van-Nostrand Reinhold.

[10] Lang, G.A. et al. 1970, "Thermal fatigue in silicon power devices", *IEEE Trans. Electron. Dev.*, Vol. 17.

[11] Suhir, E. 1999, "Modeling of thermal stress in microelectronic and photonic systems", *Future Circuits*, No. 5.

[12] Timoshenko, S. 1925, "Analysis of bi-metal thermostats", *J. Opt. Soc. Am.*, Vol. 11.

[13] Suhir, E. 2002, "Analytical stress-strain modeling in photonics engineering: Its role, attributes and interaction with the finite-element method", *Laser Focus World* (May).

[14] Ceniga, L. 2008, *Analytical Models of Thermal Stresses in Composite Materials*. New York: Nova Science Publishers.

[15] Suhir, E. 2009, "Analytical thermal stress modeling in electronic and photonic systems", *ASME Appl. Mech. Rev.*, Vol. 62, No. 4.

[16] Timoshenko, S.P. & Woinowsky-Krieger, S. 2007, *Theory of Plates and Shells*, 2nd ed. Knovel (online).

[17] Suhir, E. 1986, "Stresses in bi-metal thermostats", *ASME J. Appl. Mech.*, Vol. 55, No. 1.

[18] Suhir, E. 1999, "Adhesively bonded assemblies with identical nondeformable adherends: Predicted thermal stresses in the adhesive layer", *Composite Interfaces*, Vol. 6, No. 2.

[19] Suhir, E. 2010, "Probabilistic design for reliability", *ChipScale Reviews*, Vol. 14, No. 6.

[20] Suhir, E. & Mahajan, R. 2011, "Are current qualification practices adequate?", *Circuit Assembly* (April).

About the Authors

Dr. E. Suhir is with the University of California, Santa Cruz, CA, USA. He is a Fellow of IEEE, APS, ASME, IoP (UK) and SPE, co-founder of the ASME *Journal of Electronic Packaging* and served as its Editor-in-Chief for eight years (1993–2001). Dr. Suhir holds 22 US patents and has authored about 250 technical publications (papers, book chapters and books). He has received many professional awards, including: the 2004 ASME Worcester Read Warner Medal for establishing a new discipline: Structural Analysis of Microelectronic and Photonic Systems.

Dr. Dongkai Shangguan received his B.S. in mechanical engineering from Tsinghua University, China; his Ph.D. in materials from the University of Oxford; and his M.B.A. from San Jose State University. He conducted post-doctoral teaching at the Universities of Cambridge and Alabama, and is a guest professor at Shanghai University. Dongkai joined Flextronics International in 2001, where he is Senior Director with the Corporate Technology Group. He has 20 US and international patents and is a senior member of IEEE and SME. Dongkai has received the "Total Excellence in Electronics Manufacturing Award" from the SME.

Dr. Laurent Bechou received his Ph.D. in electronics from the University of Bordeaux 1 (France) in 1998. He then joined the Integration of Material to System Laboratory (IMS), where he has held the title of professor since 2010. His research field addresses characterization, failure mechanisms modelling and methods for reliability prediction of optoelectronic/photonic devices and systems. He is currently the manager of the "Reliability Assessment of Micro and Nano-assemblied Devices" Research Group (EDMiNA) at IMS Laboratory and the co-author of more than 80 regular papers and contributions to international conferences.

Enquiries

E. Suhir
suhire@aol.com

D. Shangguan
Dongkai.Shangguan@flextronics.com

L. Bechou
Laurent.bechou@ims-bordeaux.fr